JOURNAL OF GEOPHYSICAL RESEARCH, VOL. 88, NO. B2, PAGES 1197-1208, FEBRUARY 10, 1983

THE DYNAMIC TENSILE STRENGTH OF ICE AND ICE-SILICATE MIXTURES

Manfred A. Lange*and Thomas J. Ahrens

Seismological Laboratory, California Institute of Technology, Pasadena, California 91125

Abstract. We determined the dynamic tensile strength of ice and ice silicate mixtures at strain rates of $\sim 10^4$ s^{-1}. At these strain rates, ice has a tensile strength of ~17 MPa, and ice-silicate mixtures with 5 and 30 wt % sand content have strengths of ~20 and 22 MPa, respectively. These values lie significantly above tensile strengths of ~1.6 MPa for ice and of ~5-6 MPa for frozen silt, measured at strain rates of $\sim 10^{-2}$ to 10^{0} s^{-1}, but markedly below values found for a variety of rocks at comparable strain rates. Results of the present experiments are used to derive parameters for continuum fracturing models in icy media, which are used to determine relations between tensile strength and strain rate, and to predict stress and damage histories as well as size frequency distributions for ice and ice-silicate fragments. It is found that tensile strength σ_M is related to strain rate by $\sigma_M \propto \dot{\varepsilon}_o^{[0.25-0.3]}$, similar to results obtained for other geological materials. The increase of small fragments relative to larger fragments with increasing strain rate, as predicted by the continuum model, is a result which parallels findings in laboratory impact experiments.

Introduction

The strength of crystalline solids is dependent on the mode and rate of stress loading. Compressive and tensile strengths of many geological materials vary by as much as 1 order of magnitude when subjected to either static (strain rates of $\lesssim 10^{-3}$ s^{-1}) or dynamic (strain rates of $\gtrsim 10^{2}$ s^{-1}) tests [Grady and Hollenbach, 1979]. Knowledge of the dynamic tensile strengths of rocks is essential for an understanding of fracturing and fragmentation processes. Applications include many industrial processes involving rock breakage, such as quarrying and mining operations [Carter, 1978], impact or explosive crater formation [O'Keefe and Ahrens, 1976], and processes related to the accretion of planetary bodies [Matsui and Mizutani, 1977].

Although water ice is a common geological material, relatively little has been done to determine its mechanical properties over a wide range of stress and strain rates. Voyager discoveries of impact cratered surfaces on the satellites of Jupiter and Saturn [e.g., Smith et al., 1979, 1981] have refocused attention on the study of physical properties of ice and ice-silicate mixtures. Many of the processes related to the origin and evolution of the icy moons of Jupiter and Saturn require the knowledge of fracturing and fragmentation properties of icy substances. Our goal in previous studies has been to establish some data and scaling laws related to impact crater formation and fragmentation of ice and ice-silicate mixtures [Lange and Ahrens, 1981, 1982a, b]. A central observation, pertinent to most of these experiments, was the occurrence of tensile failure as the principal mechanism in the fragmentation of impacted icy targets.

The goal of the present study is the determination of the dynamic tensile strength of icy media at strain rates of $\sim 10^4$ s^{-1}. These data will help to understand better the macroscopic phenomena observed in our impact experiments and will be used in the derivation of scaling laws for fragmentation and crater formation in icy substances.

The dynamic tensile strength of ice and ice-silicate samples with 5 and 30 wt % sand content at temperatures between ~230 and 250 K was obtained by carrying out experiments in which plexiglas plates impacted target pellets consisting of these materials. Upon wave reflection, tensile stress pulses of $\lesssim 0.75$ μs duration and strain rates of $\sim 10^4$ s^{-1} result. The shock-loaded samples were recovered and analyzed subsequent to each experiment, and the stress at which spallation or breakage of the samples occurred was defined as the dynamic tensile strength of the substance.

We describe in the next sections the basic experimental techniques and results and attempt to use these results to model the fracturing process of icy media in terms of a continuum model.

Experimental Techniques

Sample Preparation and Assembly

All samples were prepared by compressing finely crushed ice (mean grain size ~0.1 to 0.5 mm) or ice-silicate mixtures containing specified amounts of silica sand (mean grain sizes of 0.1 to 0.5 mm) into sample pellets of 20 mm diameter and 6 mm thickness. The grain size of crushed ice was reduced using a chilled food blender. The ice powder or a homogeneous mixture of ice and silica sand was then filled in a mold and compacted by use of a hand-operated hydraulic press. During compression, the sample was evacuated, thus avoiding extensive trapping of air bubbles. This procedure gave mostly transparent or semitransparent samples with no observable void spaces. Extensive recrystallization along grain boundaries of single ice grains took place during sample compression. The sample pellets were pressed into annular stainless steel target plates which were cooled via the cooling coil circuit surrounding the sample (Figure 1). Temperatures were monitored with a thermocouple attached to the target plate, close to the sample. Since the target plate was thinner than the sample (5 mm versus 6mm, respectively) the plexiglas flyer

*Present address: Alfred-Wegener-Institut für Polarforschung, Columbus-Center, D-2850 Bremerhaven, Germany.

Paper number 2B1806.
0148-0227/83/002B-1806$05.00

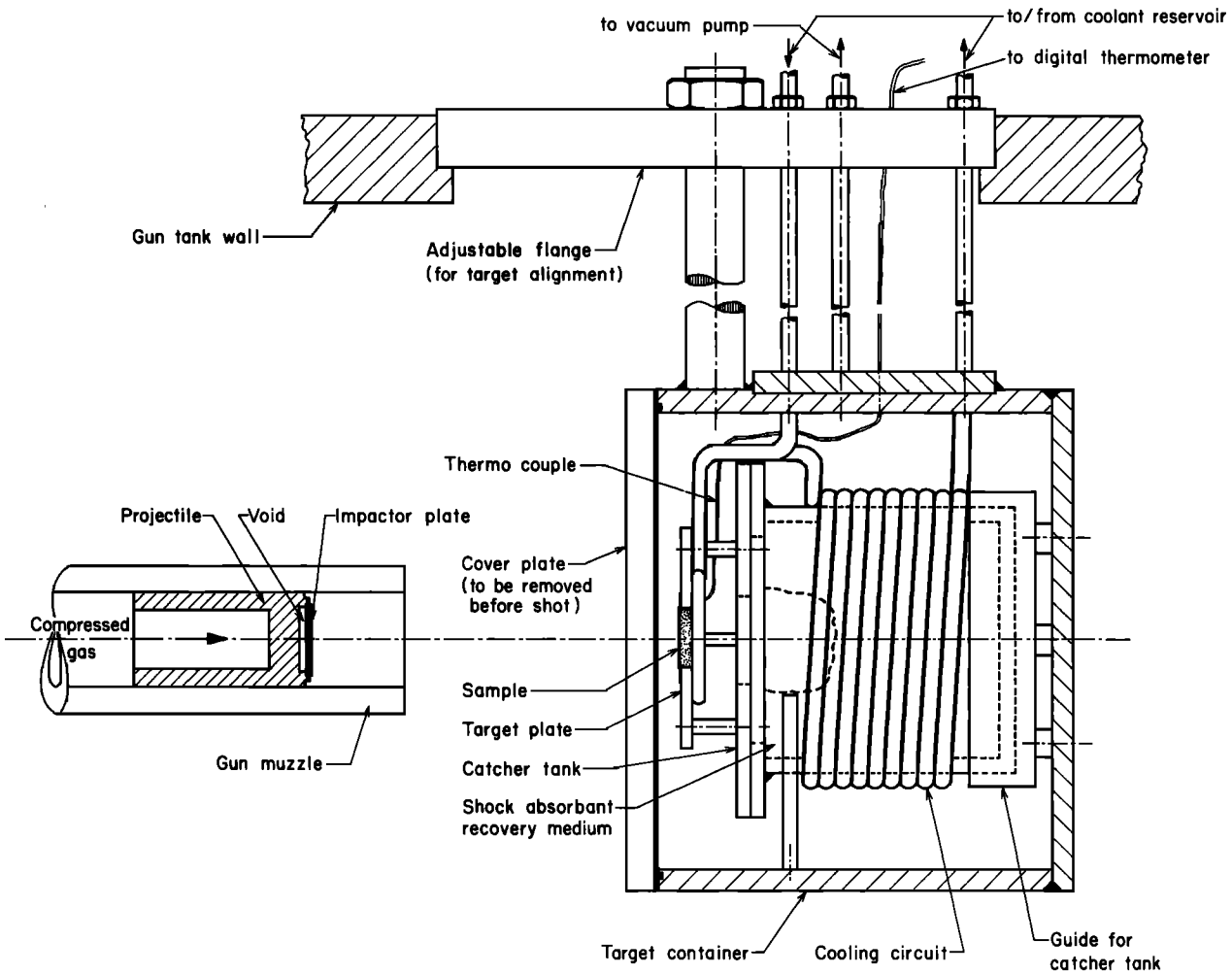

Fig. 1. Cross section of experimental assembly for measuring tensile properties of ice. The cover plate remains in place until immediately before each shot and allows evacuation of target container. Markings on the cover plate also allow alignment of the target plate with respect to the gun barrel and provide for plane impacts of the projectile into the sample.

plate could impact the sample and be stopped by the target plate.

The complete sample assembly (Figure 1) consists of the target plate attached to a steel catcher tank. An opening in the catcher tank is aligned with the target plate such that the impacted sample is driven into a cloth sack covering the opening in the tank. The sack closes itself off and is in turn driven into a mass of ice powder in the catcher tank. This avoids further damage of the sample and provides cooling of the impacted sample until recovery. The target plate and catcher tank are cooled via chilled methyl alcohol which is pumped through copper piping from a solid CO_2 and acetone bath (Figure 1). This provides sample temperatures of ~230-250 K.

The catcher tank and the attached target plate are placed in a larger aluminum target container which is aligned with the barrel of a 40 mm compressed-air gun. The target container can be closed with a plexiglas window and is evacuated until immediately prior to firing the gun. This prevents the buildup of frost layers on the sample and target plate and improves the temperature control of the sample. The window also serves as a reference for aligning the target with respect to the gun barrel. Since the target plate and sample are always at a fixed position with respect to the target container (see Figure 1), alignment of the container assures plane impact of the projectile onto the sample, a condition important in these experiments.

Experimental Procedure

Many of the experimental procedures we used are similar to those of Cohn and Ahrens [1981]. As in their experiments, a Lexan projectile carrying a plexiglas flyer plate at its front surface is accelerated by the expansion of precompressed air. Final projectile velocities varied between 4.7 and 23.3 m/s depending on the pressure of the compressed air. Projectile velocities are measured in two ways. Interruption of three laser beams, positioned at known distances along the path of the projectile, allow determination of two velocities of the accelerating projectile. The

interruption of the final laser beam and a signal of a stress gage, positioned at the target plate and activated by impact of the projectile, allow measurement of the final impact velocity.

Uniaxial tensile loading of the sample is achieved by the interaction of two relief waves traveling into the sample from free surfaces of sample and flyer [Cohn and Ahrens, 1981]. They originate as reflections of initial compression waves generated by impact of the flyer onto the sample. Knowledge of the wave velocities for compression and relief waves in both materials determines the thickness of the flyer plate to be used in order to provide a state of maximum tension approximately in the mid-plane of the sample. For tensile stresses below the strength of a sample no observable damage or only incipient spallation will result. For stresses exceeding the tensile strength, either the sample will spall in two or a few larger fragments, or complete fragmentation will occur. Analysis of the recovered sample allows an assessment of the damage done by tensile stresses, and knowledge of the projectile velocity yields the stress experienced by the sample (see below).

Determination of Experimental Parameters

A number of assumptions are made in the present study. We assume that shock and relief wave velocities U_s and U_r in sample and flyer plate can be approximated by the longitudinal elastic wave velocities of these materials. We also assumed that the tensile stress level is equal to that of the initial compression waves [see Cohn and Ahrens, 1981].

We calculate the thickness of the plexiglas flyer plates necessary to generate maximum tensile stress in the mid-plane of the samples. A necessary prerequisite is the knowledge of compressional wave velocities in flyer and sample materials. Measurements of the P wave velocities of the different sample materials are described elsewhere. The P wave velocity of plexiglas (= 2.8 km/s, density = 1.18 g/cm^3) was obtained from the study of Barker and Hollenbach [1970] (see Table 1).

For the tensile waves to meet in the mid-plane of the sample the reflected wave in the flyer plate must arrive at the sample-flyer interface when the primary compressive wave in the sample reaches the free surface of the sample. This requires the condition

$$2\frac{d_f}{C_f} = \frac{d_s}{V_p} \tag{1}$$

where C_f, V_p are the compressional wave velocities in flyer and sample, respectively, and d_f, d_s are the thicknesses of flyer and sample, respectively. With d_s = 6 mm and wave velocities as given in Table 1, d_f varies from 2.2 to 2.4 mm. For most experiments, a flyer plate thickness of 2.21 mm was used, which falls into this thickness range.

Following Cohn and Ahrens' [1981] derivation, the dynamic tensile stress σ_t in the sample is given by

$$\sigma_t = \frac{\rho_s V_p \rho_f C_f}{\rho_s V_p + \rho_f C_f} U_{pr} = K U_{pr} \tag{2}$$

TABLE 1. Sample Properties

Sand Content wt %	Sand Content vol %	Density*, g/cm^3	Ultrasonic P Velocity, km/s	K, PMMA Impact Plate, 10^6 kg m^{-2} s^{-2}
		0.917	3.83	1.70
5	1.8	0.948	3.51	1.66
30	12.9	1.141	3.65	1.84

*Bulk density for samples with zero porosity.

where ρ_s, ρ_f are sample and flyer densities, respectively. The material constants K for impacts of the present sample types with plexiglas flyer plates are given in Table 1. Multiplication of K by U_{pr} (m/s) yields the tensile stress in megapascals for each experiment (Table 2).

Cohn and Ahrens [1981] showed that the major uncertainty in K is caused by neglecting the difference between ultrasonic P wave velocities and shock velocities in the sample material. They demonstrated that, for their experiments, a variation in V_p by 10% would change the value of K by less than 2%, a fact caused mainly by the low shock impedance of plexiglas. Following their derivation, we have

$$\frac{\partial \sigma_t}{\partial V_p}\frac{V_p}{\sigma_t} = \frac{\rho_f C_f}{\rho_f C_f + \rho_s V_p} \tag{3}$$

Using the appropriate parameters for the sample material in the present study, we find that

$$\frac{\partial \sigma_t}{\partial C_s}\frac{V_p}{\sigma_t} < 0.5 \tag{4}$$

which means that variation of V_p by 10% results in changes of K by <5%. Although less favorable than Cohn and Ahrens' [1981] result, mainly caused by a lower shock impedance of our sample material as compared to rock samples, the assumption of shock velocities equal to the P velocity of the sample materials does not affect our results significantly.

The strain rate in our experiments was estimated as follows. Strain ε in shock-loaded solids is given by

$$\varepsilon = \frac{U_p}{U_s} \tag{5}$$

where U_p, U_s are the particle and shock velocity, respectively. By using first-order principles for the continuity of stress and displacement across the flyer plate-sample interface one derives an equation which gives ε as a function of known material parameters:

$$\varepsilon = \frac{\rho_f C_f}{\rho_f C_f + \rho_s V_p}\frac{U_{pr}}{V_p} \tag{6}$$

The strain rate $\dot{\varepsilon}$ is approximately given by the ratio between strain ε and the time interval Δt needed to impose tensile strain in the entire sample:

$$\Delta t = \frac{x/2}{V_p - \Delta V_p} - \frac{x/2}{V_p + \Delta V_p} \tag{7}$$

which can be written as

TABLE 2. Experimental Data

Shot No.	Sand Content, wt %	Target Temperature, °K	Projectile Velocity, m/s	Tensile Stress, MPa	Result
I-2		240	23.3	39.7	completely fragmented
I-3		229	21.9	37.3	completely fragmented
I-4		230	9.2	15.7	fragmented
I-5		245	4.7	8.0	intact, no visible cracks
I-6		242	9.5	16.2	fragmented
I-7		240	7.3	12.4	intact, no visible cracks
I-8		244	10.1	17.2	fragmented
I-9		247	8.6	14.6	intact, no visible cracks
I-10		233	9.9	16.9	spalled
IS-2	30	231	21.0	38.7	completely fragmented
IS-3	30	230	13.1	24.1	completely fragmented
IS-4	30	253	4.8	8.8	intact, incipient spall crack
IS-5	30	236	6.8	12.5	intact, no visible cracks
IS-6	30	246	8.8	16.2	intact, no visible cracks
IS-7	30	238	10.4	19.2	intact, no visible cracks
IS-8	30	248	11.8	21.7	intact, spall crack visible
IS-9	30	261	10.7	19.7	intact, no visible cracks
IS-11	30	240	12.3	22.7	intact, no visible cracks
IS-13	30	247	13.3	24.5	fragmented
IS-10	5	227	8.8	14.6	intact, no visible cracks
IS-12	5	243	9.5	15.7	intact, no visible cracks
IS-14	5	247	12.3	20.4	fragmented

$$\Delta t = \frac{x\ \Delta V_p}{V_p^2 - (\Delta V_p)^2} \qquad (8)$$

Here, x is the sample thickness. The terms $(V_p + \Delta V_p)$ and $(V_p - \Delta V_p)$ in (7) give the velocities of release waves in the stressed and stress-relieved sample, respectively; ΔV_p is the difference in sample shock velocity caused by compression of the sample, i.e, by applying a stress σ_t to the sample (see equation (2)). We evaluated ΔV_p based on data for the pressure dependence of P wave velocities in ice which yield $\partial V_p/\partial \sigma_t \simeq 7 \times 10^{-3}$ km s^{-1} MPa^{-1} [Bentley, 1975]. This gave a range of strain rates $\dot{\epsilon}$, corresponding to the range in projectile velocities, with a mean value of 2×10^4 s^{-1}.

Results

The main results of the present experiments in terms of macroscopically observable damage imposed on each sample as a result of tensile loading are given in Table 2. Four different damage categories have been defined, which are illustrated in Figure 2. The results of Table 2 are illustrated in Figure 3, where the dynamic tensile strength for each of the sample types can be determined directly. The tensile stress corresponding to the transition from intact to spalled or fragmented samples is taken as the dynamic tensile strength for each substance. We thus infer a tensile strength of 17 MPa for ice and 20 and 22 MPa for ice-sand samples with 5 and 30 wt % sand, respectively. Allowing for ±5% uncertainty in K and accounting for an experimental uncertainty in the projectile velocity by ~±0.5 m/s results in a maximum uncertainty for the tensile stresses of $\lesssim$±1 MPa (see equation (2)). The accuracy in the given tensile strengths depends on the accuracy in the tensile stress values of the experiments and on the precision with which the transition between intact and fragmented shocked samples can be determined. As can be seen in Figure 3, with the possible exception of the 5 wt % ice-sand samples, this transition can be well defined for our samples, i.e., within ±1 MPa. Thus, together with the uncertainty for the tensile stresses (±0.5 MPa), we derive a mean uncertainty for all of the materials under consideration of ±1.1 MPa for the tensile strengths.

These results, together with data for ice [Hawkes and Mellor, 1972], frozen silt [Haynes et al., 1975], which we believe is comparable to our ice-silicate samples, and ice-silicate mixtures [Goughnour and Andersland, 1968], are given in Figure 4. As can be seen, the dynamic tensile strengths of ice and ice-silicate mixtures lie well above the values found in quasi-static tests. Dynamic tensile strengths even exceed values of the compressive strength for ice and ice-silicates significantly. These results demonstrate that ice and ice-silicate mixtures, like rocks, show significantly different strength properties when stress loading is applied dynamically versus quasi-static loading. The increase in strength with increasing sand content in ice-silicate mixtures is in good agreement with results found in compression tests by Goughnour and Andersland [1968]. It also agrees with previous observations in impact cratering experiments which yielded decreasing crater dimensions with increasing sand content for a given impact [Croft et al., 1979; Lange and Ahrens, 1982a].

Those samples not fragmented in our experiments were cut diametrically, and cross sections were

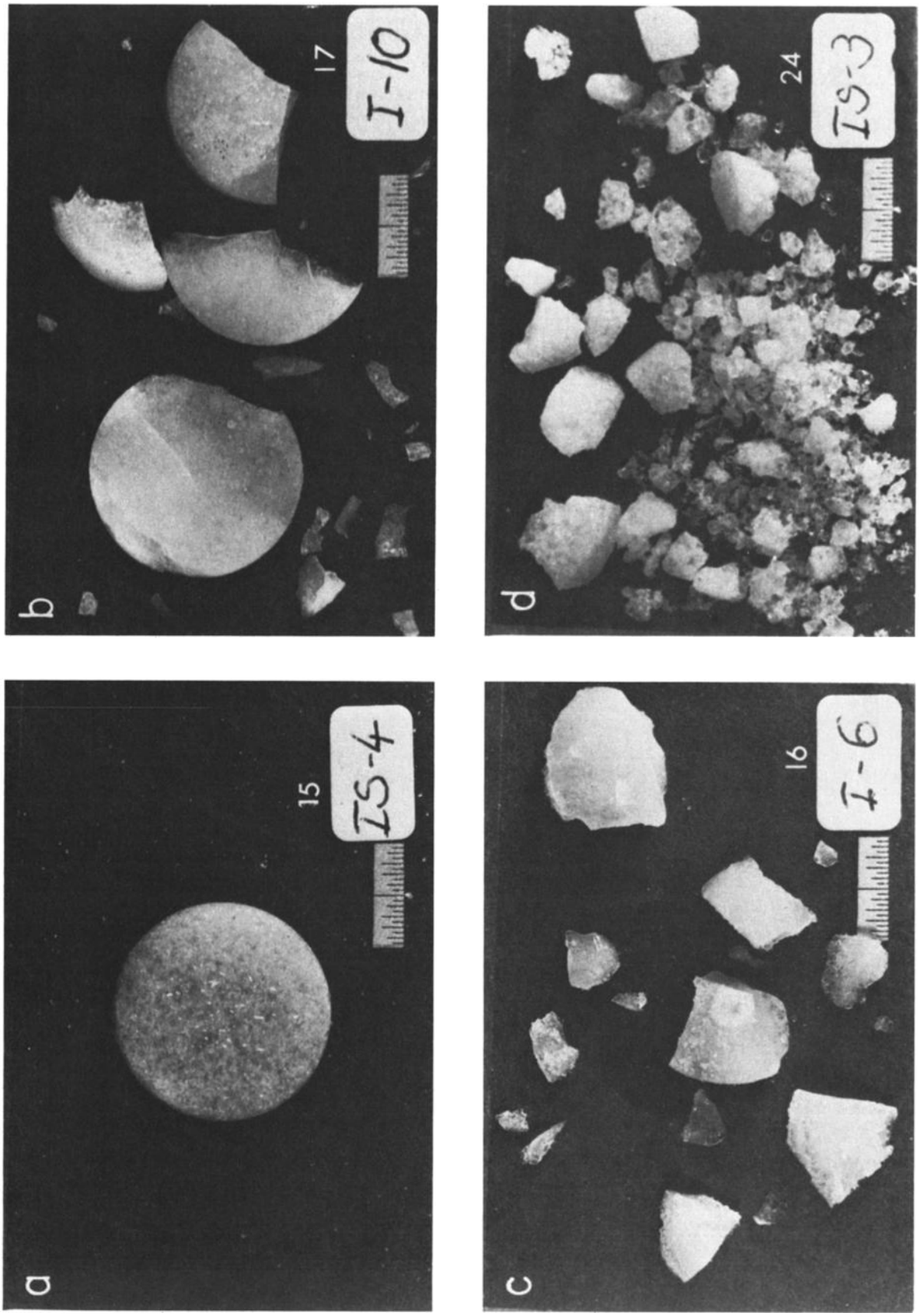

Fig. 2. Classification of sample damage due to tensile loading. Major divisions of the scales are millimeters; numbers on labels represent experiment numbers, and white numbers in lower right corners are tensile stresses in megapascals as experienced by each sample. The four classifications are (a) intact, no visible cracks, (b) spalled, (c) fragmented, and (d) completely fragmented.

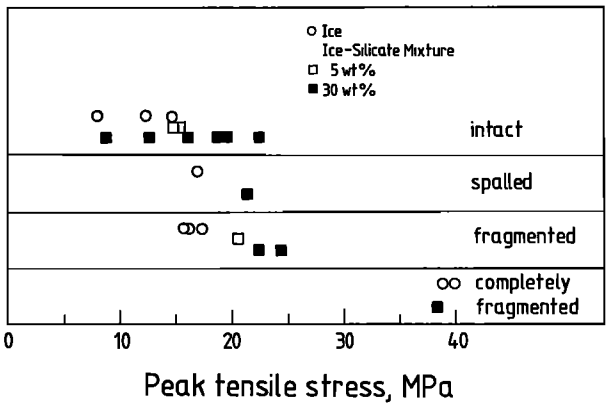

Fig. 3. Degree of fragmentation as a function of peak tensile stress. The tensile strength of each substance is determined from the stress where transition from intact to spalled or fragmented samples occurs.

investigated under a microscope. Typical examples of cross sections of each of our target types are shown in Figure 5. Of these, only one cross section, IS-4, shows clear indications of incipient fracturing; the other surface markings are artifacts of the cutting process. The fact that not more of the intact samples show signs of incipient fracturing might be explained by the rapid annealing of small cracks and fissures prior to examination [Kuroiwa, 1962].

Continuum Modeling of Fracturing in Icy Media

In order to put our results in a somewhat broader perspective and to develop limited prediction capabilities, an attempt is made to generalize our findings in terms of a continuum fracturing model [Grady and Kipp, 1980]. The two major elements in the continuum modeling of fracturing which will be applied to the present results are (1) the distribution of flaws and fissures as sources of weaknesses which lead to activation and growth of cracks under tensile loading and (2) a kinematic parameter, the rate of tensile loading of a specimen. At quasi-static loading conditions a single large crack is responsible for failure. At high rates of loading, however, a larger number of cracks is necessary to relieve the increasing tensile stress, and additional flaws must participate in the fracturing process, leading to more numerous and smaller fragments.

In the following, we will adopt most of the derivations of Grady and Kipp [1980], and only those relations essential for an understanding of the continuum model will be given here.

First, a measure of the fracture damage experienced by a stress-loaded specimen has to be defined. This parameter D, where

$$0 \leq D \leq 1 \qquad (9)$$

defines the reduction of the elastic bulk modulus K:

$$K_f = K (1 - D) \qquad (10)$$

K_f is the bulk modulus of the fractured material and defines a state of an intact (D = 0), partly fractured (0 < D < 1), and completely fragmented (D = 1) specimen. D can be described by

$$D = N V \qquad (11)$$

where N is the number of cracks per unit volume and $V = 4/3\ \pi r^3$ is the spherical region around a flaw of radius r which approximates the stress-relieved volume due to the traction-free boundary associated with each crack.

The activation of cracks is described by a two-parameter Weibull distribution, an approach which provides a satisfactory description of brittle fracture in crystalline solids [Jaeger and

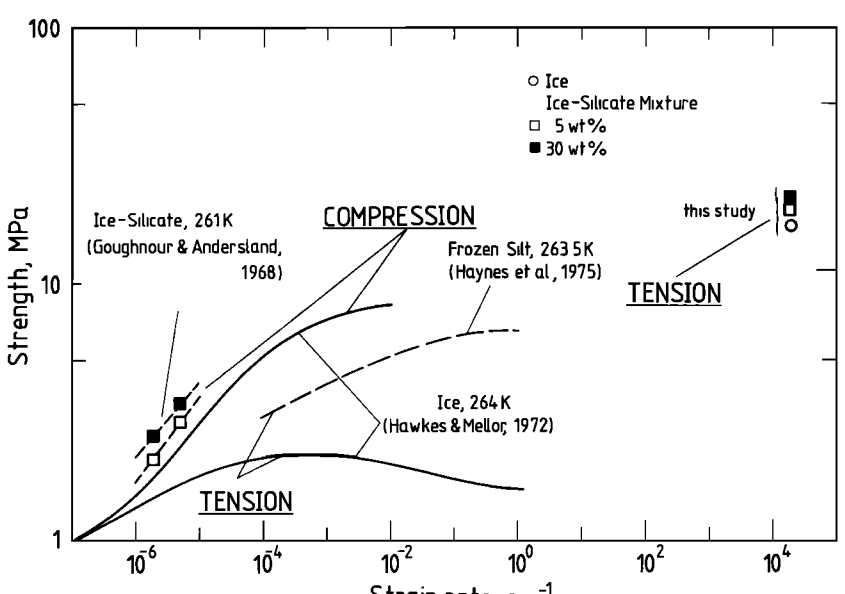

Fig. 4. Compressive and tensile strengths as a function of strain rate for icy substances. The data of Goughnour and Andersland [1968] are for ice-sand mixtures with 5 (open symbols) and 30 wt % (solid symbols) sand content.

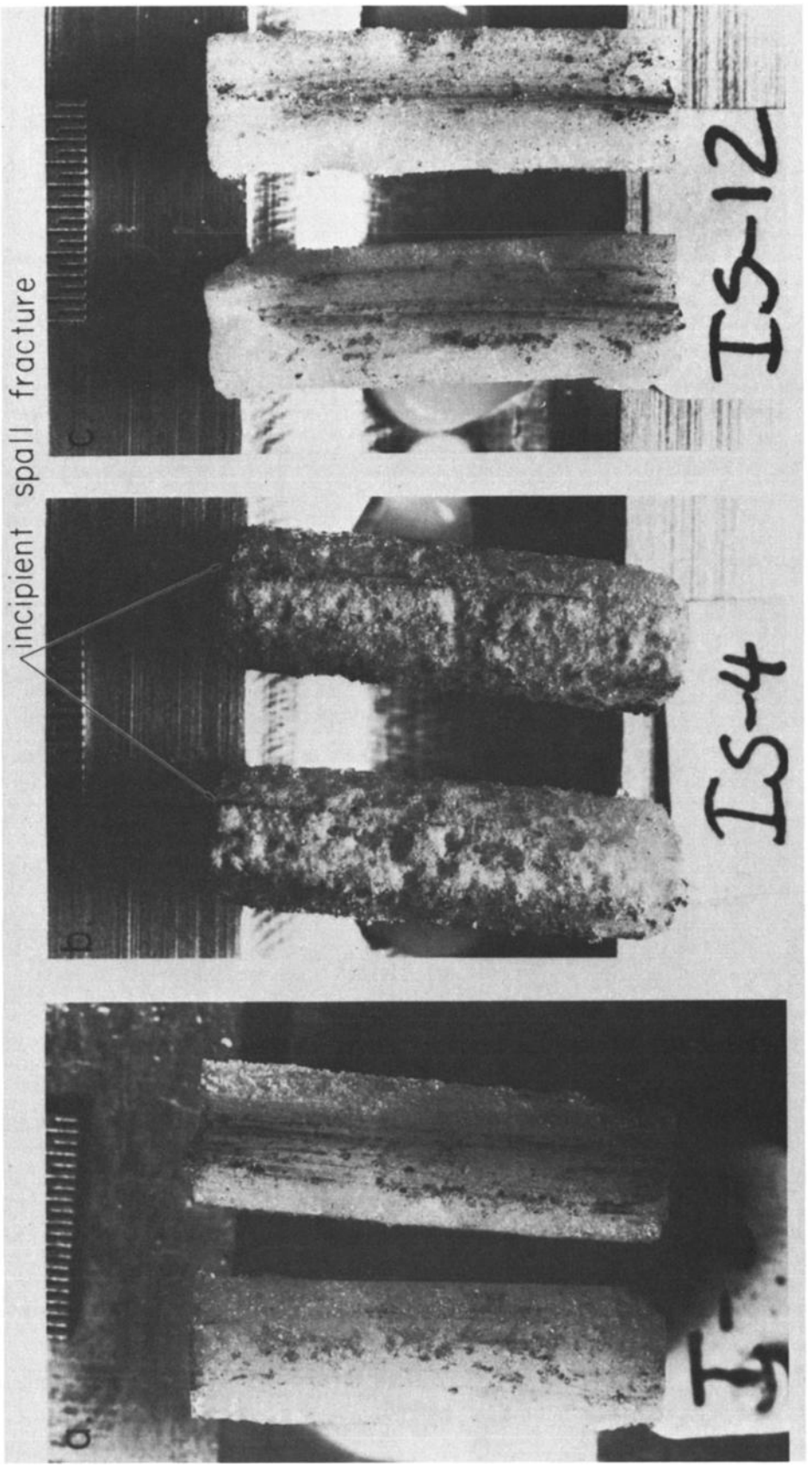

Fig. 5. Cross sections of intact, shocked samples. The main divisions on the scales are millimeters, and the numbers designate sample numbers. Only the sample IS-4 shows indications of incipient spall. Figures 5a, 5b, and 5c show ice and ice-silicate samples with 30 and 5 wt % sand, respectively.

Cook, 1979, pp. 199-201]. The number of flaws, n, which are activated at or below a tensile strain level ε is given by

$$n = k\,\varepsilon^m \tag{12}$$

where k and m are material parameters.

The growth of an activated flaw is assumed to proceed at a constant velocity C_g. Thus, the increase in the stress-relieved volume V surrounding this crack as a function of time t is given by

$$V(t) = 4/3\,\pi\,(C_g\,t)^3 \tag{13}$$

For the case of constant strain rate loading, i.e., $\varepsilon(t) = \dot{\varepsilon}_o t$, Grady and Kipp [1980] derive an equation which relates the damage growth D(t) to time t and constant strain rate $\dot{\varepsilon}_o$:

$$D(t) = \alpha \dot{\varepsilon}_o^m\, t^{m+3} \tag{14}$$

where

$$\alpha = \frac{8\pi\, C_g^{\,3}\, k}{(m+1)(m+2)(m+3)} \tag{15}$$

On the basis of this relation, the stress history $\sigma(t)$, the maximum or fracture strength σ_M, the time at which maximum stress accumulation is reached, t_M, and the time at which failure occurs, t_f, can be obtained from

$$\sigma(t) = K\,\dot{\varepsilon}_o\, t\,(1-\alpha\,\dot{\varepsilon}_o^m\, t^{m+3}) \tag{16}$$

$$\sigma_M = K\,(m+3)(m+4)^{-(m+4)/(m+3)}\,\alpha^{-1/(m+3)}\,\dot{\varepsilon}_o^{\,3/(m+3)} \tag{17}$$

$$t_M = (m+4)^{-1/(m+3)}\,\alpha^{-1/(m+3)}\,\dot{\varepsilon}_o^{\,-m/(m+3)} \tag{18}$$

$$t_f = \alpha^{-1/(m+3)}\,\dot{\varepsilon}_o^{\,-m/(m+3)} \tag{19}$$

Finally, Grady and Kipp [1980] derive relations which allow determination of a fragment size distribution F(L) and the dominant fragment size L_M for constant strain rate loading:

$$F(L) = \frac{\pi m k L^3}{12\,C_g}\,(t_f - L/2\,C_g)^{m-1}\,\dot{\varepsilon}_o^m \tag{20}$$

$$L_M = \frac{6\,C_g}{m+2}\,\alpha^{-1/(m+3)}\,\dot{\varepsilon}_o^{\,-m/(m+3)} \tag{21}$$

The principal variable in the relations (14)-(21) is the strain rate $\dot{\varepsilon}_o$; major parameters are the velocity of crack growth C_g, the material parameters m and k in the Weibull distribution (equation (12)), and the bulk modulus K. The bulk modulus can be obtained from the measured P wave velocities V_p (M. A. Lange, unpublished data, 1982) in each of our sample types by

$$K \simeq \tfrac{5}{9}\,\rho\,V_p^{\,2} \tag{22}$$

where the assumption is made that the shear wave velocity $V_s \simeq \sqrt{3}\,V_p$ [Bullen, 1976, p. 75].

Grady and Kipp [1980] find values for k, m, and C_g for oil shale by fitting equations (17) and (21) to experimental data which relate principal fragment size L_M and fracture stress σ_M to strain rates. They find that C_g is about 0.4 times the P wave velocity of oil shale, a result in good agreement with data of Shockey et al. [1974], who find $C_g \sim 1/3\,V_p$ for Arkansas novaculite. We assume that this relation holds for most crystalline solids and define

$$\tfrac{1}{3}\,V_p \leq C_g \leq \tfrac{2}{5}\,V_p \tag{23}$$

for our sample materials.

The remaining parameters needed to define a continuum fracturing model for ice and ice-silicate mixtures are the constants k and m (equation (12)). We used the following conditions to estimate values for these parameters: (1) the values of the tensile strengths σ_M for each of our target materials at a strain rate $\dot{\varepsilon}_o$, of 2×10^4 s^{-1}, (2) the principal fragment size L_M in completely fragmented samples, (3) the total duration of the tensile stress pulse in the samples, and (4) the tensile strength of ice at a strain rate of 10^0 s^{-1} [Hawkes and Mellor, 1972].

The principal fragment size L_M was found by measuring the long axis of some 200 fragments of shots I-2 (Figure 6a) and IS-2 (Figure 6b) on photographs taken of the fragments directly after the experiment. The lack of data for smaller fragments is due to the limit in the resolution of the photographs. On the basis of these measurements we define as the principal fragment size, i.e., the size range which covers the majority of the measured particles, $0.1 \leq L_M \leq 0.35$ mm for the present experiments, i.e., for a strain rate of 2×10^4 s^{-1}. Although this size range encompasses the mean sizes of the ice and sand grains from which our samples were made, we do not believe that L_M simply reflects the initial grain sizes. As mentioned above, our methods of sample preparation provided ample recrystallization of ice in the sample pellets.

The duration of tensile stress pulses $\Delta\tau$ in the experiments varies between ~0.3 and 0.75 μs, depending on the peak tensile stress reached in the samples. This can be used to constrain the times at which maximum stress is reached in the sample (t_M, equation (18)) and the time at which failure occurs (t_f, equation (19)) by requiring that t_M, $t_f \lesssim \Delta\tau$.

The tensile strength of ice at a strain rate of 10^0 s^{-1} lies at ~1.6 MPa [Hawkes and Mellor, 1972]. Since there are no tensile strengths for ice-silicate mixtures with relatively low sand contents, as distinct from ice-saturated sand data available, we assume that the ratios between tensile strengths of ice and those of ice-silicate mixtures are approximately independent of strain rate. This allows us, based on our measurements at 2×10^4 s^{-1} and the tensile strength of ice at 10^0 s^{-1}, to estimate strength values for ice-silicate mixtures at a strain rate of 10^0 s^{-1}, which yields values of 1.88 MPa and 2.07 MPa for ice-silicates with 5 and 30 wt % sand, respectively. The tensile strength for frozen silt at 10^0 s^{-1} (~6 MPa [Haynes et al., 1975]) is used as an upper bound for the strength of our ice silicate samples at a strain rate of 10^0 s^{-1}.

We varied the parameters m and k for each sample type systematically and used a computer program to compute σ_M, L_M, t_M, and t_f for strain rates of 2×10^4 and 10^0 s^{-1} until that combination of m and k was found which gave satisfactory agreement of the numerically derived values with those obtained in our experiments or from sources in the literature. Figure 7 illustrates the ranges of values of σ_M for ice computed for $6 \leq m \leq 10$ and $0.32 \times 10^{40} \leq k \leq 0.32 \times 10^{50}$ at a strain rate of 2×10^4 s^{-1}. The values of $m = 8.7$ and $k = 0.32 \times 10^{45}$ gave the

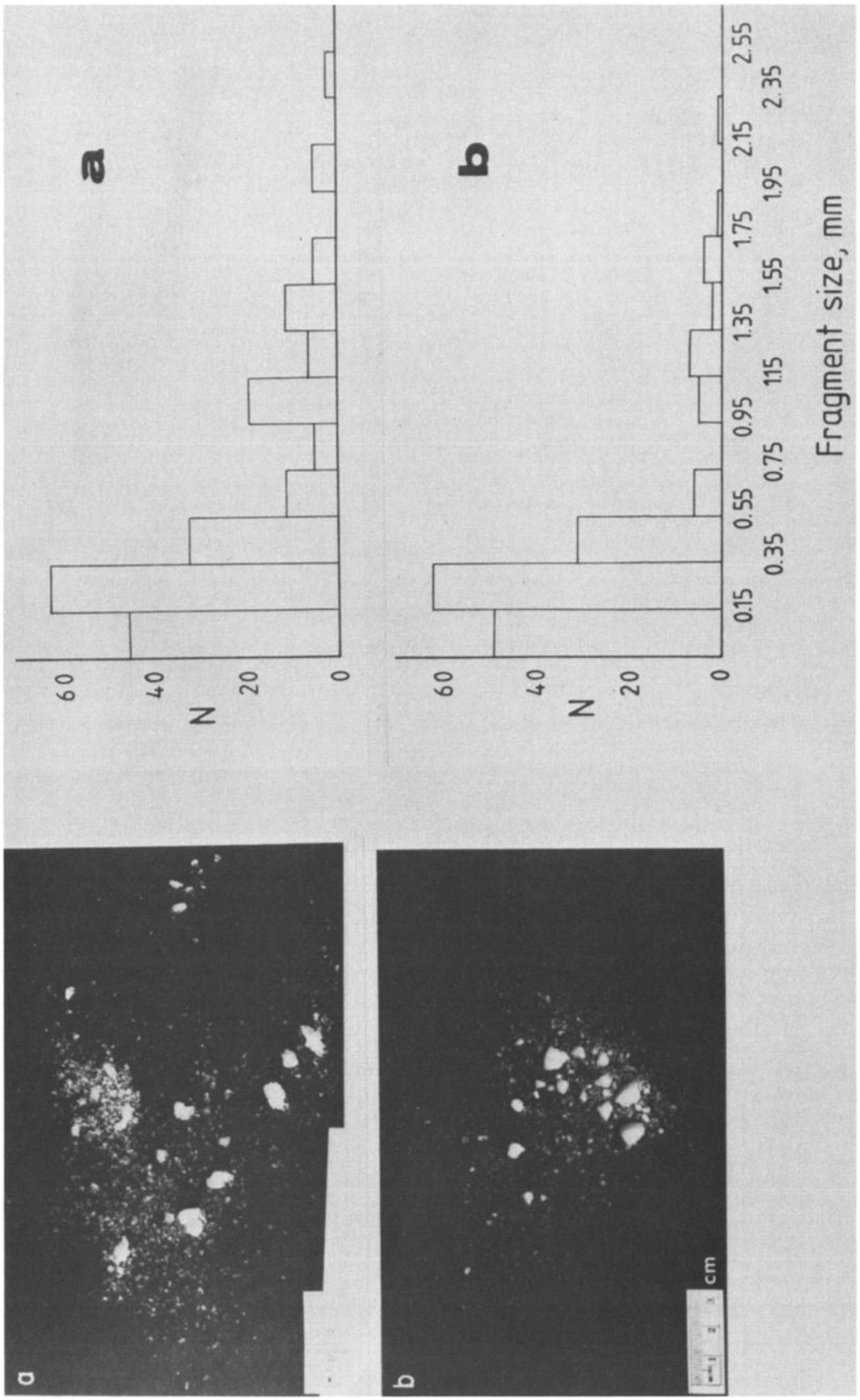

Fig. 6. Photographs of completely fragmented (a) ice (I-2) and (b) ice-silicate samples (IS-2) and size distribution of some 200 fragments as determined by measuring fragment sizes on photographs. The scale in both photographs is in centimeters.

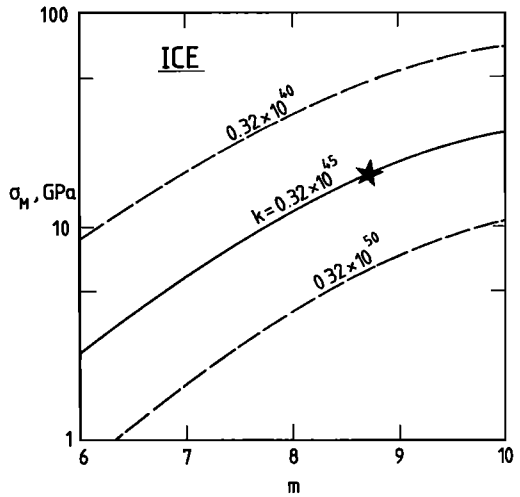

Fig. 7. Tensile strength σ_M versus parameter m (for different values of k) as obtained numerically in continuum modeling of the fracturing process in ice at a strain rate of 2 x 10^4 s^{-1}. The star marks that combination of m and k which gave the closest agreement between observed and predicted fracturing parameters.

most satisfactory agreement of σ_M (= 17.5 MPa) with the value obtained in our experiment (= 17 MPa) as well as with respect to the other criteria mentioned above. Table 3 gives the values of m and k for all of the present sample materials and the values of σ_M, L_M, t_M, and t_f as computed by use of equations (17)-(19) and (21). As can be seen, the fits between computed and measured material parameters in Table 3 for each combination of k and m can be made quite close. This suggests that the continuum fracturing model provides a useful tool in evaluating and generalizing experimental fracturing data in icy media.

Discussion and Conclusions

The parameters derived in the previous section (Table 3) can now be used to predict fracturing behavior of icy media and related properties. Figure 8 gives fracture stresses (tensile strengths) for each of the materials under consideration as a function of strain rate. Following the results of Grady and Hollenbach [1979] and Grady and Kipp [1980], we propose a relation between tensile strength σ_M and stress rate $\dot{\varepsilon}_o$ in icy media:

$$\sigma_M \propto \dot{\varepsilon}_o^{[0.25-0.3]} \qquad (24)$$

which is close to relations found for other geological materials [Grady and Kipp, 1980]. Also given are tensile strengths for a number of different rocks, as obtained in similar experiments [Cohn and Ahrens, 1981; Cohn et al., 1982], which lie well above the strength values for icy media.

The continuum fracturing model also allows computation of stress and damage histories during tensile loading (equations (14)-(16)). Damage growth is negligible until a critical time (= t_M) at which damage growth becomes catastrophic. This

TABLE 3. Continuum Fracturing Model Parameters for Icy Media: Comparison of Model and Observed Fracture Characteristics.

Sand Content, wt %	$\dot{\varepsilon}_o$, s^{-1}	m	k	C_g, km/s	K, GPa	σ_{M1}, MPa		L_M, mm		t_{M1}, μs		T_{f1}, μs	
						Observed	Theoretical	Observed	Theoretical	Observed	Theoretical	Observed	Theoretical
0	1	8.7	0.32×10^{45}	1.53	9.47	1.60	1.40		1.7×10^{2}		1.6×10^{2}		2×10^{2}
	2×10^{4}	8.7	0.32×10^{45}	1.53	9.47	17.0	17.5	0.1-0.5	0.11	<0.3-0.75	0.10	<0.3-0.75	0.12
5	1	9.4	0.56×10^{44}	1.41	6.50	1.88*	1.85		2.8×10^{2}		3.1×10^{2}		3.8×10^{2}
	2×10^{4}	9.4	0.56×10^{44}	1.41	6.50	20.0	20.3	0.1-0.5	0.15	<0.3-0.75	0.17	<0.3-0.75	0.21
30	1	9.4	0.56×10^{45}	1.46	8.44	2.07*	2.00		2.4×10^{2}		2.5×10^{2}		3.1×10^{2}
	2×10^{4}	9.4	0.56×10^{45}	1.46	8.44	22.0	21.7	0.1-0.5	0.13	<0.3-0.75	0.14	<0.3-0.75	0.17

*Derived from value of σ_M for ice and the ratios of σ_M for ice to those of ice-silicates at $\dot{\varepsilon}_o = 2\times10^4$ s^{-1} as measured in present experiments.

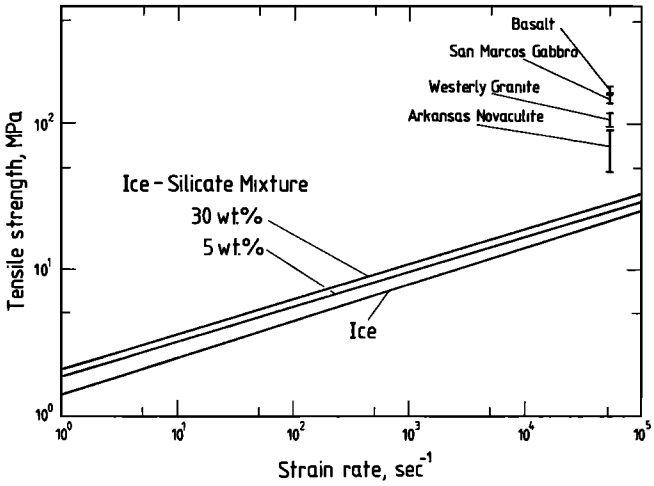

Fig. 8. Tensile strength versus strain rate for icy substances. The curves are theoretical predictions based on a continuum fracturing model for ice and ice-silicates. The tensile strengths for four different rock types represent results of shock wave experiments by Cohn et al. [1982] (San Marcos Gabbro) and Cohn and Ahrens [1981] (others) at strain rates between 10^4 and 10^5 s^{-1}.

corresponds to a gradual increase in tensile stress to a maximum (fracture stress) at which the drop-off in stress proceeds rapidly. Increase in strain rate results in shifts of $\sigma(t)$ and $D(t)$ curves to shorter periods of times; i.e., t_M and t_f decrease (see Figure 4 of Grady and Kipp [1980]).

The size distribution of fragments resulting from the complete fragmentation of icy substances can be computed as a function of strain rate from equation (19). We observe trends qualitatively similar to those found by Grady and Kipp [1980] (see their Figure 5). With increasing strain rate, the number of small fragments relative to the number of larger fragments increases, and the principal fragment size L_M decreases (see Table 3). This agrees with impact fragmentation experiments on ice and ice-silicate mixtures which demonstrate an increase in the number of small fragments relative to large fragments with increasing impact velocity (strain rate) [Lange and Ahrens, 1981, also unpublished manuscript, 1982].

Dynamic strength values for ice and ice-silicate mixtures lie significantly above values found in quasi-static tests. This is surprising in the case of ice, since previous [Hawkes and Mellor, 1972] measurements over a relatively wide range of strain rates ($\sim 10^{-5}$ to 10^0 s^{-1}) suggested an independence of tensile strength on strain rate.

Acknowledgments. We appreciate the skillful help of E. Gelle, W. Ginn, and M. Long in the experiments. Special thanks to T. Feng, who spent many hours of sample preparation in the cold lab. The use of the cold lab facility and helpful advice proffered by B. Kamb are appreciated. Careful reviews by S. K. Croft and M. Cintala are gratefully acknowledged. M. Lange is supported by a stipend from the Deutsche Forschungsgemeinschaft. Work was supported under NASA grant NGL-05-002-105. Contribution 3806, Division of Geological and Planetary Sciences, California Institute of Technology.

References

Barker, L. M., and R. E. Hollenbach, Shock wave studies of PMMA, fused silica and sapphire, J. Appl. Phys., 41, 4208-4226, 1970.

Bentley, C. R., Advances in geophysical exploration of ice sheets and glaciers, J. Glaciol., 15, 113-135, 1975.

Bullen, K. E., Introduction to the Theory of Seismology, 381 pp., Cambridge University Press, New York, 1976.

Carter, W. J., Explosively produced fracture of oil shale, Prog. Rep. LA-7357-PR, Los Alamos Sci. Lab., Los Alamos, N. M., Nov. 1978.

Cohn, S. N., and T. J. Ahrens, Dynamic tensile strength of lunar rock types, J. Geophys. Res., 86, 1794-1802, 1981.

Cohn, S. N., M. A. Lange, and T. J. Ahrens, Dynamic spall strength of San Marcos Gabbro (abstract), Eos Trans. AGU, 63, 441, 1982.

Croft, S. K., S. W. Kieffer, and T. J. Ahrens, Low-velocity impact craters in ice and ice-saturated sand with implications for Martian crater count ages, J. Geophys. Res., 84, 8023-8032, 1979.

Goughnour, R. R., and O. B. Andersland, Mechanical properties of a sand-ice system, J. Soil Mech. Found. Div. Am. Soc. Civ. Eng., 94, 923-959, 1968.

Grady, D. E., and R. E. Hollenbach, Dynamic fracture strength of rock, Geophys. Res. Lett., 6, 73-76, 1979.

Grady, D. E., and M. E. Kipp, Continuum modelling of explosive fracture in oil shale, Int. J. Rock Mech. Min. Sci. Geomech. Abstr., 17, 147-157, 1980.

Hawkes, I., and M. Mellor, Deformation and fracture of ice under uniaxial stress, J. Glaciol., 11, 103-131, 1972.

Haynes, F. D., J. A. Karalius, and J. Kalafut, Strain rate effect on the strength of frozen silt, USA CRREL Res. Rep. 350, U. S. Army Cold Reg. Res. Eng. Lab., Hanover, N. H., 1975.

Jaeger, J. C., and N. G. W. Cook, Fundamentals of Rock Mechanics, 593 pp., Chapman and Hall, London, 1979.

Kuroiwa, D., A study of ice sintering, USA CRREL Res. Rep. 86, U. S. Army Cold Reg. Res. Eng. Lab., Hanover, N. H., 1962.

Lange, M. A., and T. J. Ahrens, Fragmentation of ice by low velocity impact, Proc. Lunar Planet. Sci. Conf. 12th, 1676-1687, 1981.

Lange, M. A., and T. J. Ahrens, Impact cratering in ice- and ice-silicate targets: An experimental assessment (abstract), Lunar Planet. Sci., XIII, 415-416, 1982a.

Lange, M. A., and T. J. Ahrens, Impact fragmentation of ice-silicate bodies (abstract), Lunar Planet. Sci., XIII, 417-418, 1982b.

Matsui, T., and H. Mizutani, Why is a minor planet minor? Nature, 270, 506-507, 1977.

O'Keefe, J. D., and T. J. Ahrens, Impact ejecta on the moon, Proc. Lunar Sci. Conf. 7th, 3007-3025, 1976.

Shockey, D. A., D. R. Curran, L. Seaman, J.

T. Rosenberg, and C. F. Petersen, Fragmentation of rock under dynamic loads, Int. J. Rock Mech. Min. Sci., 11, 303-317, 1974.

Smith, B. F., L. A. Soderblom, R. Beebe, J. Boyce, G. Briggs, M. Carr, S. A. Collins, A. F. Cook, G. E. Danielson, M. E. Davies, G. E. Hunt, A. Ingersoll, T. V. Johnson, J. McCauly, H. Masursky, T. Owen, C. Sagan, E. M. Shoemaker, S. Strom, V. E. Suomi, and J. Veverka, The Galilean satellites and Jupiter: Voyager 2 imaging science results, Science, 206, 927-950, 1979.

Smith, B. F., L. A. Soderblom, R. Beebe, J. Boyce, G. Briggs, A. Bunker, S. A. Collins, C. F. Hansen, T. V. Johnson, J. L. Mitchell, R. J. Terrille, M. Carr, A. F. Cook, J. Cuzzi, J. B. Pollack, G. E. Danielson, A. Ingersoll, M. E. Davies, G. Hunt, H. Masursky, E. M. Shoemaker, D. Morrison, T. Owen, C. Sagan, J. Veverka, J. Strom, and V. E. Suomi, Encounter with Saturn: Voyager 1 imaging science results, Science, 212, 163-191, 1981.

(Received August 12, 1982;
revised November 11, 1982;
accepted November 19, 1982.)